Finite Particle Method for Progressive Failure Simulation of Truss Structures

Ying Yu[1]; Glaucio H. Paulino, M.ASCE[2]; and Yaozhi Luo, M.ASCE[3]

Abstract: A structural analysis framework called the finite particle method (FPM) for structure failure simulation is presented in this paper. The traditional finite-element method is generated from continuum mechanics and the variational principle; vector mechanics form the basis of FPM. It discretizes the domain with finite particles whose motions are described by Newton's second law. Instead of imposing a global equilibrium of the entire continuous system, FPM enforces equilibrium on each particle. Thus, particles are free to separate from one another, which is advantageous in the simulation of structural failure. One of the features of this approach is that no iterations to follow nonlinear laws are necessary, and no global matrices are formed or solved in this method. A convected material frame is used to evaluate the structure deformation and internal force. The explicit time integration is adopted to solve the equation of motion. To simulate the truss structure failure, a failure criterion on the basis of the ideal plastic constitutive model and a failure modeling algorithm are proposed by using FPM. According to the energy conservation study of a two-dimensional (2D) truss, the energy is decomposed and balanced during the failure process. Also, a more complicated three-dimensional (3D) structure failure simulation is given. The comparison of the simulation results and the practical failure mode shows the capability of this method. **DOI: 10.1061/(ASCE)ST.1943-541X.0000321.**

CE Database subject headings: Structural failures; Progressive collapse; Conservation; Simulation; Trusses.

Author keywords: Finite particle method; Vector mechanics; Explicit time integration; Failure model; Progressive failure; Energy conservation.

Introduction

Structural progressive failure behavior attributable to unexpected loads, such as a typhoon, an earthquake, and impact loads, has been an area of great interest for a long time. However, it is complicated and costly to investigate such phenomena by means of theoretical studies and experiments. Therefore, the numerical simulation becomes an essential complementary way to analyze structural progressive failure.

The finite-element method (FEM) derived from the variational principle and continuum mechanics has been widely used in an extensive range of engineering problem analyses in the past few decades. However, progressive failure behavior involves strong nonlinearities and discontinuities; and thus, viable alternatives to the standard FEM need to be considered. The FEM generated from the variational principle imposes a global equilibrium from the entire continuous system and reduces the force residual at nodes. These unbalanced nodal forces may introduce some nonzero work under rigid body motion and may cause inaccuracies in the solution or even failure of the computation because of the singularity of the stiffness matrix. However, the FEM, with special treatments and modifications, has been applied to progressive failure simulations. For instance, Lynn and Isobe (Lynn and Isobe 2007a) implemented the ASI-Gauss technique into finite-element codes and simulated the impact collapse of framed structures. By introducing extrinsic cohesive model and topological data structure into the FEM, dynamic fracture and crack microbranching processes were successfully simulated (Zhang et al. 2007). An arbitrary Lagrangian-Eulerian formulation, such as the particle finite-element method (PFEM) (Onate et al. 2004) or the least squares finite-element method (LSFEM) (Oliver and Hermann 2005), could solve fluid-structure interaction problems.

On the other hand, the mesh-free approaches, benefiting from the discrete analytical model, do not have the limitations in the simulation of failure problems as the conventional FEM. The discrete-element method (DEM) (Cundall and Strack 1979) discretized a material by using rigid elements of simple shapes that interacted with one another. It could model and simulate the nonlinear and discrete behavior of particulate material such as sand and concrete (Tavarez and Plesha 2007). Particle methods such as smoothed particle hydrodynamics (SPH) (Monaghan 1992) and the moving particle semi-implicit (MPS) method (Koshizuka et al. 1998), which can model fluids and other geomaterials, have also been applied to simulate fragmentation, structural large deformations, and failures. However, these mesh-free methods require detailed models for the analysis domain and are usually computationally expensive. Therefore, these methods are more suitable for particulate materials behavior analysis rather than truss structure failure simulation.

[1]Visiting Scholar, Dept. of Civil and Environmental Engineering, Univ. of Illinois at Urbana-Champaign, 205 North Mathews Ave., Urbana, IL 61801; and Ph.D. Candidate, Space Structures Research Center, Zhejiang Univ., 388 Yuhangtang Rd., Hangzhou, China 310027. E-mail: yuying123@gmail.com

[2]Professor, Dept. of Civil and Environmental Engineering, Univ. of Illinois at Urbana-Champaign, 205 North Mathews Ave., Urbana, IL 61801 (corresponding author). E-mail: paulino@illinois.edu

[3]Professor, Space Structures Research Center, Zhejiang Univ., 388 Yuhangtang Rd., Hangzhou, China 310027. E-mail: luoyz@zju.edu.cn

Note. This manuscript was submitted on October 28, 2009; approved on September 12, 2010; published online on September 22, 2010. Discussion period open until March 1, 2012; separate discussions must be submitted for individual papers. This paper is part of the ***Journal of Structural Engineering***, Vol. 137, No. 10, October 1, 2011. ©ASCE, ISSN 0733-9445/2011/10-1168–1181/$25.00.

In contrast to the FEM and other mesh-free methods, the finite-particle method (FPM) (Yu 2010) *is derived from vector mechanics* (Ting et al. 2004)This method models the domain composed by finite particles instead of a continuous mathematical body and uses Newton's second law to describe the motions of all particles. It does not derive the equilibrium equations for stresses from variational principles as does FEM. Instead, it enforces the equilibrium at each particle, making the nodal internal force and external force balanced all the time.

The FPM can be qualified as a particle method because particles carry structural variables such as mass, density, stress, and velocity. But particles do not have physical volumes, and they are connected by elements. By using the convected material frame (Shih et al. 2004), the internal force of a particle is obtained from the deformation of the corresponding elements with which it is connected. The explicit time integration is adopted for solving the particle motion equation. Recently, Ting's mechanical concept and theory has been successfully applied to the motion analysis of planar framed structures (Wu et al. 2006), kinematically indeterminate bar assemblies (Yu and Luo 2009a), deployable structures (Yu and Luo 2009b), planar solids (Wu et al. 2008), and three-dimensional (3D) membrane structures (Wu and Ting 2008).

The motivation of this work is to establish a general finite-particle method (FPM) framework for solving truss structural failure problems. As a particle method, it is possible to add or delete particles and elements in the FPM analysis domain, which is important in the simulation of structural failure. Furthermore, every item in the basic equation of motion is clearly expressed, and the unknown displacement is solved explicitly. No iterations are necessary to follow nonlinear laws, and no global matrices are formed.

The remainder of this paper is organized as follows. The fundamentals of FPM are described, including the discretization of the structure, the basic particle motion equations, the internal force calculation, the explicit time integration, and solution procedures. The nonlinear and dynamic behaviors of a star dome truss are analyzed to prove the accuracy and generality of the FPM. A failure criterion on the basis of the ideal plastic constitutive model is proposed. Moreover, the modeling of truss structural failure in the FPM is explained, followed by an energy conservation study of the progressive failure of a simple two-dimensional (2D) truss structure. Also, a more complicated 3D truss structure example is described. Finally, some concluding remarks of this work are provided.

Finite-Particle Method

Taking the 3D bar element as an example, the fundamentals of the FPM are described in this section, including the discretization of structure, the basic particle motion equations, the internal force calculation, the nonlinear constitutive model, the explicit time integration, and solution procedures. A verification example is also presented in this section.

Discretization of Structure

In FPM, a truss structure, such as the one shown in Fig. 1(a), can be discretized with particles and elements, as shown in Fig. 1(b). It is assumed that the structural mass concentrates at particles, whereas elements have no mass and are in static equilibrium during motion. So the particle force can be obtained from the deformations of the corresponding elements with which it is connected. If the element is represented by a couple of forces, the structure can be modeled, as shown in Fig. 1(c).

Particle Motion Equations

An arbitrary particle, α, undergoes a discrete motion path, $t_0, t_1, t_2, \ldots, t_n$, with the position vector changing from $\boldsymbol{x}_0, \boldsymbol{x}_1, \boldsymbol{x}_2, \ldots$, to $\boldsymbol{x}_n$, as shown in Fig. 2. The time interval is very small, so variables such as stress and strain can be regarded as fixed for the duration of the time step and only changed at the boundary of the time step.

The motion of Particle α in a general structure follows Newton's second law:

$$m_\alpha \ddot{\boldsymbol{d}} = \boldsymbol{F}^{\text{ext}} - \boldsymbol{F}^{\text{int}} \tag{1}$$

where m_α = mass of α; $\boldsymbol{d}$ = displacement vector; $\ddot{\boldsymbol{d}}$ = acceleration vector; and $\boldsymbol{F}^{\text{ext}}$ = summation of the external forces acting on Particle α, which can be either physical forces or equivalent forces defined by mathematical concepts. The even distribution of mass from each member to the node is used in the determination of particle force, m_α. The term $\boldsymbol{F}^{\text{int}}$ denotes the summation of the internal nodal forces exerted by the elements connected with the Particle α. The formulations for internal forces of the element will be derived in the following subsection.

If the damping force is considered, the motion equation can be expressed as

$$m_\alpha \ddot{\boldsymbol{d}} = \boldsymbol{F}^{\text{ext}} - \boldsymbol{F}^{\text{int}} - \boldsymbol{F}^{\text{dmp}} \tag{2}$$

where the damping force $\boldsymbol{F}^{\text{dmp}} = \mu m_\alpha \dot{\boldsymbol{d}}$; μ = damping factor, which is the same as the definition in the dynamic relaxation method (Lewis 1984). Only the structure damping is considered. From Eq. (2), every particle is found to be in a dynamic equilibrium state under internal, external, and damping forces.

Considering the truss structure modeled by a 3D bar element, as shown in Fig. 1, each particle has only three translation degrees of freedom. The motion equation of Particle α can be expressed as

$$m_\alpha \begin{bmatrix} \ddot{d}_x \\ \ddot{d}_y \\ \ddot{d}_z \end{bmatrix} = \begin{bmatrix} f_x^{\text{ext}} \\ f_y^{\text{ext}} \\ f_z^{\text{ext}} \end{bmatrix} - \begin{bmatrix} f_x^{\text{int}} \\ f_y^{\text{int}} \\ f_z^{\text{int}} \end{bmatrix} - \begin{bmatrix} f_x^{\text{dmp}} \\ f_y^{\text{dmp}} \\ f_z^{\text{dmp}} \end{bmatrix} \tag{3}$$

Internal Force Calculation

To calculate internal forces, consider the 3D bar element shown in Fig. 3. The position vectors of the end Nodes 1 and 2 of this element at time t_a and $t_b (= t_a + \Delta t)$ are defined as $(\boldsymbol{x}_1^a, \boldsymbol{x}_2^a)$ and

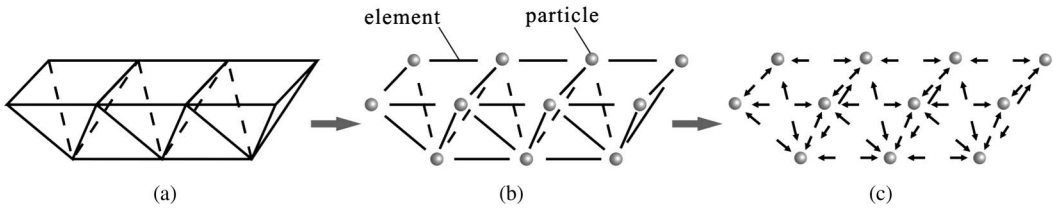

Fig. 1. (a) 3D-framed structure; (b) discretization of structure by particles and elements; (c) particles and forces

J. Struct. Eng. 2011.137:1168-1181.

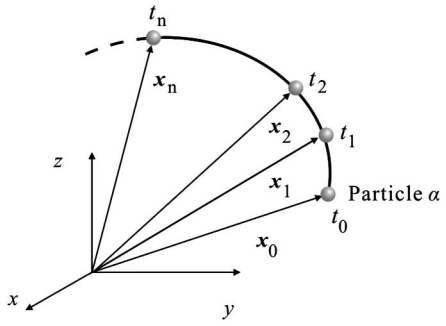

Fig. 2. Discrete motion path of Particle α

$(\boldsymbol{x}_1^b, \boldsymbol{x}_2^b)$, respectively, as shown in Fig. 3(a). The reference configuration for stress analysis of Element 12 at time t_b is set to be its configuration at t_a. So the effect attributable to the geometric change within time step Δt can be neglected. The relative displacement at Nodes 1 and 2 between time t_a and t_b are $\Delta \boldsymbol{x}_1 = \boldsymbol{x}_1^b - \boldsymbol{x}_1^a$ and $\Delta \boldsymbol{x}_2 = \boldsymbol{x}_2^b - \boldsymbol{x}_2^a$, as shown in Fig. 3(b). Then, taking the motions of Node 1 as the rigid body translations of the element, the relative displacements of Node 2 to Node 1 between the reference configuration and the current configuration is $\Delta \boldsymbol{u}_2 = \Delta \boldsymbol{x}_2 - \Delta \boldsymbol{x}_1$.

Because the internal forces are related only to the deformation, it is necessary to remove rigid body translations and rotations from the relative displacements. A simple kinematic formulation, the convected material frame (Shih et al. 2004), is suggested. First, assume the Element $1'2'$ at t_b is subjected to a fictitious translation, $-\Delta \boldsymbol{x}_1$, and a fictitious reversed rotation, $-\Delta\theta$. Then, Element $1'2'$ is displaced to Position $1''2''$, as shown in Fig. 4(a). The internal force is obtained at this configuration. The relative rigid body displacement attributable to the fictitious rotation $V\boldsymbol{u}_2^r$ can be obtained as follows (Goldstein et al. 2002):

$$V\boldsymbol{u}_2^r = -(\boldsymbol{R}^T - \boldsymbol{I})\Delta \boldsymbol{x}' \tag{4}$$

where $\boldsymbol{I} = 3 \times 3$ unit matrix; $\boldsymbol{R}$ = rotation matrix of $\Delta\theta$; $\Delta\theta$ = angle between Elements 12 and $1'2'$; $\Delta \boldsymbol{x}'$ = position vector of Node 2 in the local deformation coordinate at time t_b; and $\Delta \boldsymbol{x}' = [l_{1'2'} \quad 0 \quad 0]$ where $l_{1'2'}$ = length of Element 12 at time t_b. Therefore, the deformation displacement increment of Element 12 from t_b to t_a is

$$\Delta \boldsymbol{u}_2^d = \Delta \boldsymbol{u}_2 + \Delta \boldsymbol{u}_2^r = \Delta \boldsymbol{x}_2 - \Delta \boldsymbol{x}_1 - (\boldsymbol{R}^T - \boldsymbol{I})\Delta \boldsymbol{x}' \tag{5}$$

The time segment Δt is assumed to be very small, and the deformation during the time step is infinitesimal. Therefore, the infinitesimal strain and engineering stress could be used to evaluate stress. As a bar element, its deformation is related only to the variation of the bar length. Thus, instead of using Eq. (5), the incremental deformation of a bar can be determined from the following equation:

$$\Delta \boldsymbol{u}_2^d = (l_{1'2'} - l_{12})\boldsymbol{e}_{12} \tag{6}$$

where l_{12} and $l_{1'2'}$ = length of Element 12 at time t_a and t_b, respectively; and $\boldsymbol{e}_{12}$ = directional vector of Element 12 at time t_a.

After the fictitious rotation, Element $1''2''$ is parallel to Element 12 [Fig. 4(b)], which satisfies the basic assumptions of material mechanics. The axial force of the element is

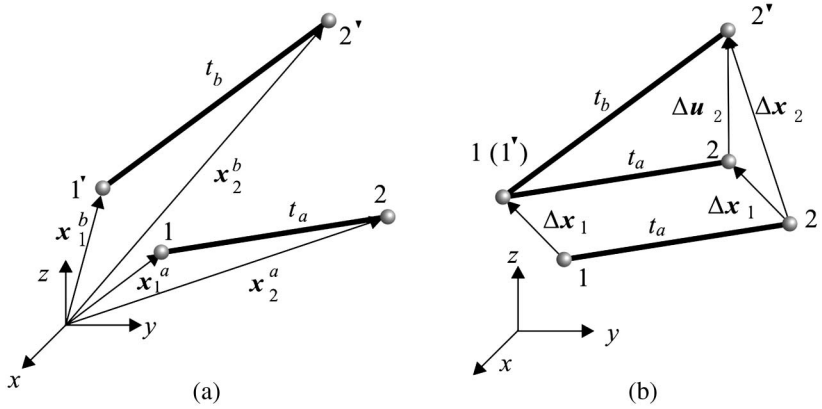

Fig. 3. Single 3D bar element: (a) displacements of particles at two ends of element; (b) relative displacements of particles

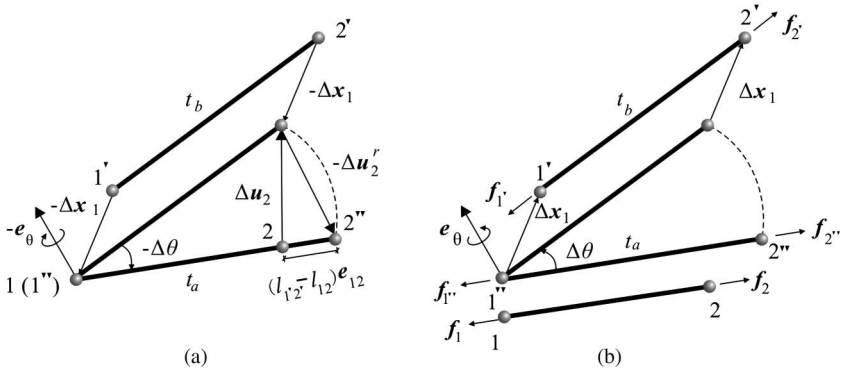

Fig. 4. Particle internal force calculations: (a) reversed rotation, $-\Delta\theta$, and translation, $-\Delta x_1$; (b) rotation, $\Delta\theta$, and translation, Δx_1

J. Struct. Eng. 2011.137:1168-1181.

$$\boldsymbol{f}_{2''} = \boldsymbol{f}_a + \Delta\boldsymbol{f}_a = \left[\sigma_\alpha A_\alpha + \frac{E_\alpha A_\alpha}{l_{12}}(l_{1'2'} - l_{12})\right]\boldsymbol{e}_{12} \tag{7}$$

where $\boldsymbol{f}_a$ = axial force of Element 12 at time t_a; $\Delta\boldsymbol{f}_a$ = incremental axial force of Element 12 at time t_b; σ_a = axial stress at time t_a; E_a = Young's modulus; and A_a = section area of Element 12. According to the static equilibrium condition

$$\boldsymbol{f}_{1''} = -\boldsymbol{f}_{2''} \tag{8}$$

As the axial force at the fictitious position is obtained, let the element subject to a rotation, $\Delta\theta$, and a translation, $\Delta\boldsymbol{x}_1$, return to its original position. In this process, only the direction of the element axial force is changed. Then the real element axial force can be determined [Fig. 4(b)]:

$$\boldsymbol{f}_{2'} = -\boldsymbol{f}_{1'} = \left[\sigma_\alpha A_\alpha + \frac{E_\alpha A_\alpha}{l_{12}}(l_{1'2'} - l_{12})\right]\boldsymbol{e}1'2' \tag{9}$$

where $\boldsymbol{e}_{1'2'}$ = directional vector of Element 12 at time t_b. The axial force $\boldsymbol{f}_{1'}$ and $\boldsymbol{f}'_2$ is applied to the corresponding particle, respectively. The internal force of a particle can be identified by the summation of all axial forces of elements connected to it.

Nonlinear Constitutive Model

Eq. (9) is the internal force formulation for a linear constitutive model. Because structural "failure" directly is bound up with the nonlinear property of the structural material, the inelastic constitutive model is also considered in the analysis (Yu 2010). In the FPM, material nonlinearity does not cause nonlinearity to the particle motion equation. It only causes differences in the calculation of the particle internal force.

Consider a nonlinear constitutive model, $\sigma = E(\varepsilon)$, in the analysis. The strain-stress relationship and loading-unloading state of the bar element should be determined first in every time step according to the element state in the last time step. Then, the incremental axial force of the bar element in Eq. (7) can be determined by $\sigma = E(\varepsilon)$ explicitly because the incremental deformations of the last step are already known. The internal forces of particles connected to the element are changed correspondingly. Therefore, the only difference between linear and nonlinear constitutive models in the FPM is how the particle internal force is calculated.

Explicit Time Integration

Several methods can be employed to find solutions for the particle motion equations [see Eq. (2)]. Because every item at the right-hand side can be expressed explicitly and also because the iteration in the solution procedure is avoided in doing so, explicit time integrations are used. If a simple central difference is adopted, the velocity and acceleration can be approximated as

$$\dot{\boldsymbol{d}}_n = \frac{1}{2\Delta t}(\boldsymbol{d}_{n+1} - \boldsymbol{d}_{n-1}) \tag{10}$$

$$\ddot{\boldsymbol{d}}_n = \frac{1}{\Delta t^2}(\boldsymbol{d}_{n+1} - 2\boldsymbol{d}_n + \boldsymbol{d}_{n-1}) \tag{11}$$

where $\boldsymbol{d}_{n+1}$, $\boldsymbol{d}_n$, and $\boldsymbol{d}_{n-1}$ = displacement of an arbitrary particle at step $n+1$, n, and $n-1$, respectively; and Δt = constant time increment. Substituting Eqs. (10) and (11) into Eq. (2) yields

$$\boldsymbol{d}_{n+1} = \left(\frac{2}{2+\mu\Delta t}\right)\frac{\Delta t^2}{m_\alpha}(\boldsymbol{F}_n^{\text{ext}} - \boldsymbol{F}_n^{\text{int}}) + \left(\frac{4}{2+\mu\Delta t}\right)\boldsymbol{d}_n - \left(\frac{2-\mu\Delta t}{2+\mu\Delta t}\right)\boldsymbol{d}_{n-1} \tag{12}$$

Eq. (12) is a simple and explicit formula, from which displacements of structures can be determined.

Computational Procedures

The computational procedure of the FPM for bar assemblies is very simple. It can be summarized as follows:

1. At the first time step, $t_0 = 0$, give all initial input information, such as the initial displacements, external force, and constraint conditions. According to Eq. (12), $\boldsymbol{d}_{-1}$ is needed, which can be obtained from the following equation:

$$\boldsymbol{d}_{-1} = \boldsymbol{d}_0 - \Delta t\dot{\boldsymbol{d}}_0 + \frac{1}{2}\Delta t^2\ddot{\boldsymbol{d}}_0 \tag{13}$$

   Substituting $\boldsymbol{d}_{-1}$, $\boldsymbol{d}_0$, $\boldsymbol{F}_0^{\text{ext}}$, and $\boldsymbol{F}_0^{\text{int}}$ into Eq. (12), $\boldsymbol{d}1$ is determined. Store $\boldsymbol{d}0$ and $\boldsymbol{d}1$; then, move forward to the next step.
2. At any time step, $n(n \neq 0)$, update the positions of all particles first.
3. Determine the new axial force of each element at its new position by using Eqs. (6)–(9). If the nonlinear constitutive model is considered, the incremental internal force is obtained by the nonlinear stress-strain relationship of the nonlinear constitutive model. Assemble them for each particle internal force, $\boldsymbol{F}_n^{\text{int}}$.
4. If particle external forces, $\boldsymbol{F}_n^{\text{ext}}$, are changed at time step t_n, update them.
5. If particle mass values, m_α, are changed at time step t_n, update them.
6. Substituting $\boldsymbol{d}_{n-1}$, $\boldsymbol{d}_n$, $\boldsymbol{F}_n^{\text{ext}}$, and $\boldsymbol{F}_n^{\text{int}}$, into Eq. (12), $\boldsymbol{d}_{n+1}$ is determined. Store $\boldsymbol{d}_n$ and $\boldsymbol{d}_{n+1}$; then, move forward to the next step, t_{n+1}.
7. If time is less than the ending time, return to Step 2. Otherwise, stop.

The analytical code was developed in Matlab, and all examples in this work were computed with a personal computer (i.e., 2.6 GHz Pentium Dual-Core CPU and 2 GB RAM with the Windows XP operating system).

Example

The star dome truss shown in Fig. 5 is a commonly used benchmark problem for testing the accuracy of different geometric and material nonlinear algorithms (Driemeier et al. 2005; Leu and Yang 1990; Papadrakakis 1981). Papadrakakis combined the dynamic relaxation and the first-order conjugate gradient methods in the investigation of the large deflection analysis. Leu and Yang generated the results of the truss nonlinear behavior analysis by considering the effects of both the rigid body motion and stretching. Driemeier et al. explored the various features of this structure with plasticity and damage by using the nonlinear finite-element method. However, without any special treatments, the FPM was used to analyze the nonlinear and dynamic behavior of this truss with the same program used in the linear static analysis, which could prove the accuracy and generality of this method.

The structure properties are shown in Fig. 5. The cross-section area of all members is 20 mm^2.

J. Struct. Eng. 2011.137:1168-1181.

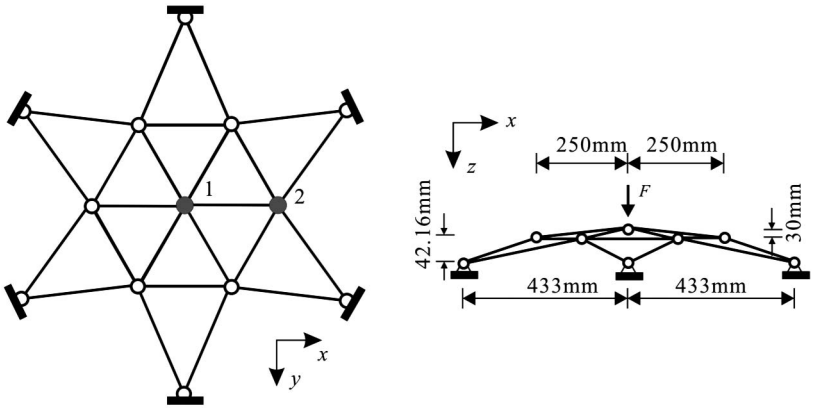

Fig. 5. Star dome truss geometry and loading

To catch the buckling property of this dome, a displacement control of the FPM was used. Eq. (12) turns to be

$$\boldsymbol{F}_n^{\text{ext}} = \left(\frac{2+\mu\Delta t}{2}\right)\frac{m_\alpha}{\Delta t^2}\left[\boldsymbol{d}_{n+1} + \left(\frac{2-\mu\Delta t}{2+\mu\Delta t}\right)\boldsymbol{d}_{n-1} - \left(\frac{4}{2+\mu\Delta t}\right)\boldsymbol{d}_n\right] + \boldsymbol{F}_n^{\text{int}} \tag{14}$$

As the displacement increases, the external force, F in Fig. 5, could be obtained directly from Eq. (14). The bilinear kinematic hardening model used in the Driemeier et al. research was adopted for this example. The Young's modulus at the linear elastic and hardening phases are 200 GPa and 200 MPa, respectively. The yield stress $\sigma^{\text{crit}} = 250$ Mpa. Set the time step $\Delta t = 1 \times 10^{-5}$ s and the displacement incremental step $\Delta d = 1 \times 10^{-6}$ mm. Fig. 6 shows the elastic and plastic pre- and postbuckling behaviors of load versus displacement at Nodes 1 and 2. The elastic and plastic limit loads of 4,662N and 3,033N were predicted for this analysis, which are quite similar to the Driemeier et al. results.

To catch the dynamic buckling property of this dome, Eq. (12), as a force control method, can be used directly in the analysis. Apply constant forces $F = 3{,}630N$, 3,631N, 3,632N, and 3,633N to the elastic model, respectively. The vertical displacement responses of Node 1 are shown in Fig. 7(a). When $F > 3{,}632N$, the deflection of Node 1 vibrates with a very small amplitude. When $F > 3{,}632N$, the structural buckling happens, and the deflection of Node 1 becomes much larger. Thus, the dynamic snap-through load is approximately 3,632N. Comparing to the static result 4,662N, the dynamic ultimate load of the star dome truss is reduced by 22% in these analyses. Similarly, Kassimali and Bidhendi (1988) analyzed the 24-rod truss and found the dynamic stability elastic ultimate load dropped by 24% compared with static results. The vertical plastic displacement responses of Node 1 versus different constant loads are shown in Fig. 7(b). The dynamic plastic ultimate load approximately of 2,255N is reduced 26% compared to the static plastic result. The dynamic plastic analysis takes approximately 0.375 s of computer time for a physical time of 0.04 s.

Failure Criterion for Truss Structure

Most of the work reported in the literature uses the stress or strain limit as a truss structure failure criterion. That is, if the strain or stress in a certain member exceeds the limit value of the material, fracture happens, and this member cannot support the stress or strain any longer. In this paper, a failure criterion for the truss structure is proposed on the basis of the ideal plastic constitutive model.

Moments usually induce bending and shearing forces into members. Because a 3D bar element is used in this paper, the code can not simulate the bending and shearing failure in a single element. To modify this point, compression also is considered to

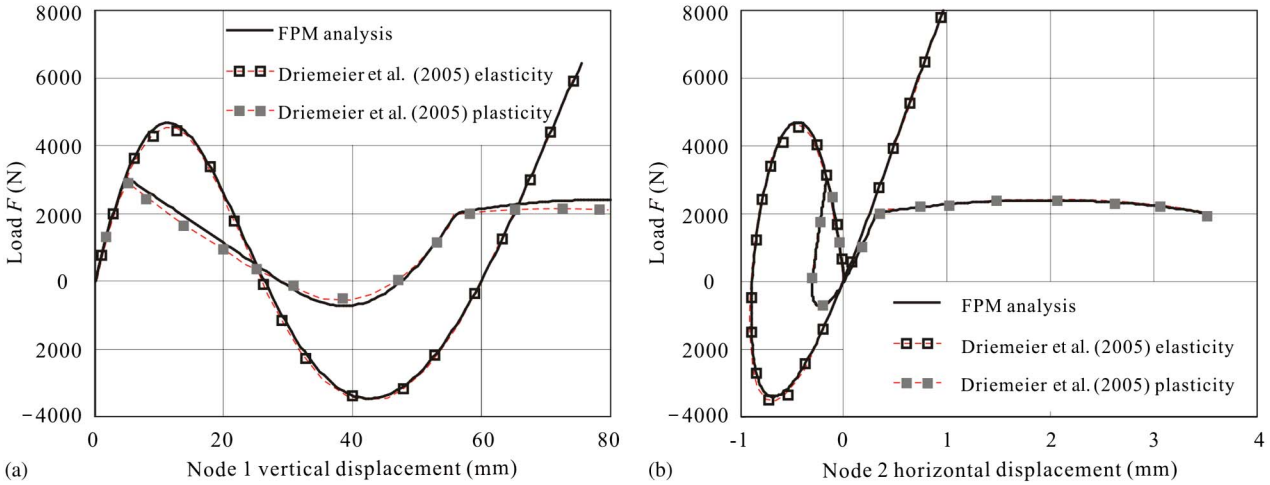

Fig. 6. Star dome truss displacement results: (a) load versus vertical displacement of Node 1; (b) load versus horizontal displacement of Node 2

J. Struct. Eng. 2011.137:1168-1181.

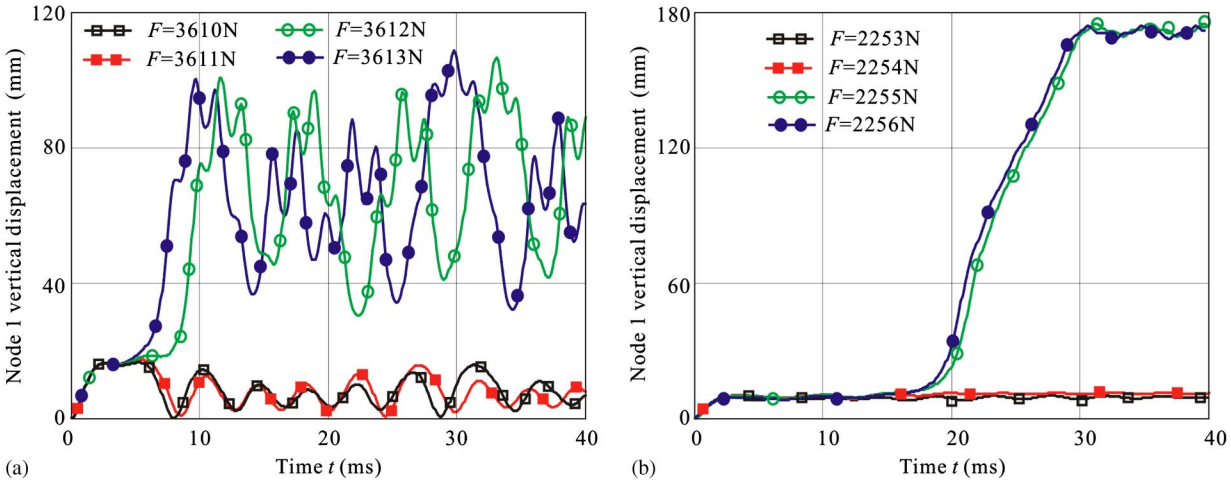

Fig. 7. Star dome truss dynamic displacement results of Node 1 versus different constant loads: (a) elasticity; (b) plasticity

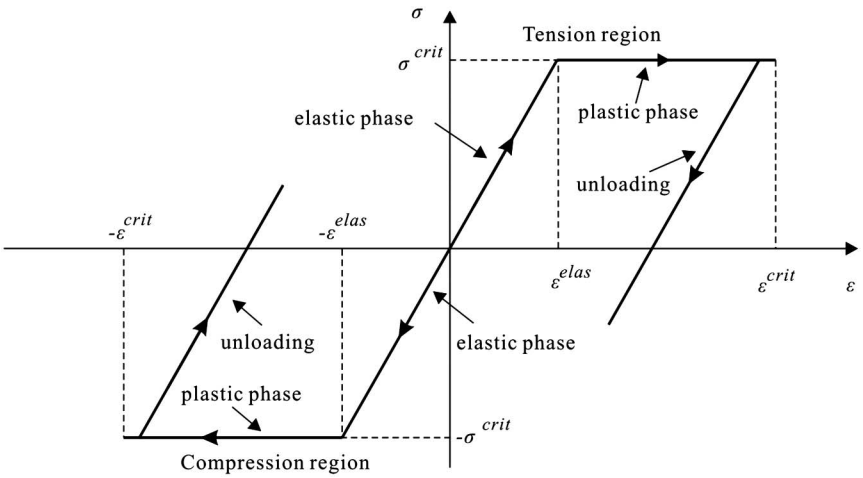

Fig. 8. Ideal-plastic stress-strain curve for failure criterion

be one reason that element failures can result. As shown in Fig. 8, the relationship between stress and strain is linear until the member axial tensile or compressive stress reaches the material's yield value, σ^{crit}. Then, the material behavior is proposed to be plastic until failure happens. However, the exact critical strain value at the point at which failure happens is not quite clear. According to several experiments, the critical axial tensile strain value is suggested to be approximately three times the yield strain, $\varepsilon^{\text{crit}} = 3\varepsilon^{\text{elas}}$ (Lynn and Isobe 2007b).

After failure happens, the fracture member may have one or two free ends. If the external force is not exerted, unloading will occur in the failure member. The unloading is elastic in nature with the same slope as the initial loading phase, also shown in Fig. 8.

FPM for Modeling Truss Structure Failure

When a structure reaches the failure criterion, member fracture and crack are unavoidable. Because the FPM model is a particle discretization domain, and no continuum is assumed, it could handle the discontinuous structure naturally after failure happens. In this study, a simple and straightforward method for modeling truss structure failure is introduced.

Fig. 9(a) shows part of a truss structure modeled by a 3D bar element. If Member AB reaches the failure criterion, fracture may happen at A, B, or both. To determine the fracture position, the particle force at both member ends, $\boldsymbol{f}_A$ and $\boldsymbol{f}_B$ must be calculated. Comparing these two particle forces, if $|\boldsymbol{f}_A| > |\boldsymbol{f}_B|$, fracture happens at A. Then Element $A'B$ is departed from Particle A. A new particle is generated at A', as shown in Fig. 9(b). If $|\boldsymbol{f}_A| < |\boldsymbol{f}_B|$, fracture happens at B; then, a new particle is generated at B', as shown

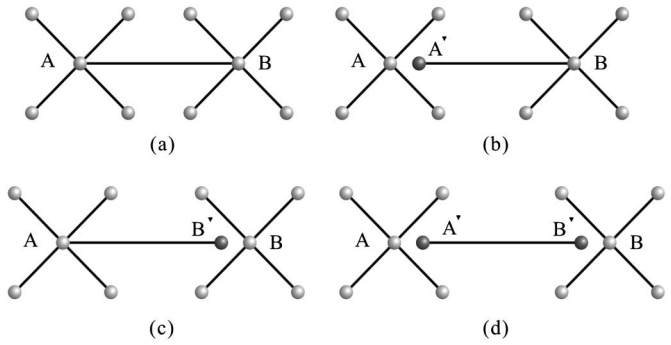

Fig. 9. FPM for modeling member failure

J. Struct. Eng. 2011.137:1168-1181.

in Fig. 9(c). If $|f_A| = |f_B|$, fracture happens at both ends. Element $A'B'$ will be departed from the remaining structure and become a free element. Two new particles, A' and B', are generated simultaneously, as shown in Fig. 9(d).

When the fracture happens, the basic computational procedure of the FPM will not be changed. Only the properties of both the newly added particles and the corresponding original particles should be updated. Assuming the fracture of Element AB happens at A [see Fig. 9(b)], the following procedure is adopted to perform the adaptivity:

1. The mass of the newly generated particle depends on the element connected to it. Half of the mass of Element $A'B$ is redistributed to Particle A'. Correspondingly, the mass of the new Particle A' should be subtracted from the mass of Particle A.
2. With the new topology information, particle forces still depend on the forces of elements connected to them. The internal force of Particle A' can be evaluated from the deformation of Element $A'B$; the internal force of Particle A can be identified by the summation of all the axial forces of elements connected to it. The external forces of Particle A' and A are evaluated in the same way.
3. The total number of elements will not be changed, whereas the total number of particles should be updated at the point at which the fracture happens.

Regardless of which case in Figs. 9(b) and 9(c) happens in the fracture analysis, the motions of all particles still can be obtained by Eq. (12) with updated forces and masses.

Energy Conservation During Failure Process

In FPM, the explicit time integration with the central difference method is adopted for solving the motion equations. Krenk (2006) demonstrated that the response calculated by the Newmark-based time integration algorithm satisfies the energy balance equation. During the complicated failure process, a large deformation and fracture of the truss structure induces strong nonlinearity and discontinuity. However, the energy conservation should still be observed.

The external work is done by external forces. It is the summation of the external work done by the external force exerted on each particle over this particle displacement, given by

$$W_e = \sum_{n=1}^{N_p} f_n^{\text{ext}} \Delta_n \tag{15}$$

where f_n^{ext} = external force on Particle n; Δ_n = displacement of Particle n; and N_p = total number of particles.

The internal work includes kinetic energy, strain energy, and damping work. The kinetic energy is attributable to particle velocity, which is the summation of the kinetic energy of every particle, given by

$$W_k = \sum_{n=1}^{N_p} \frac{m_n v_n^2}{2} \tag{16}$$

where m_n = mass of Particle n; and v_n = velocity of Particle n.

The strain energy is attributable to the deformation of elements. Because the truss structure in this paper is modeled by the 3D bar element, the deformation is only related to the length variation of the element. According to the stress-displacement curve shown in Fig. 8, the element may undergo an elastic phase, a plastic phase, or unloading. Taking the tension part as an example, it could be specified as three cases to get the strain energy, as shown by the shaded regions in Fig. 10.

If the tensile element is in an elastic phase, as shown in Fig. 10(a), the single element strain energy w_n is given by

$$w_n = \frac{1}{2} \int \sigma_B \varepsilon_B dV \tag{17}$$

where σ_B and ε_B = stress and strain at Point B, respectively.

If the tensile element is in a plastic phase, as shown in Fig. 10(b), w_n is given by

$$w_n = \int \left(\sigma^{\text{crit}} \varepsilon_B - \frac{1}{2} \sigma^{\text{crit}} \varepsilon^{\text{crit}} \right) dV \tag{18}$$

where σ^{crit} = yield stress; and $\varepsilon^{\text{crit}}$ = yield strain.

If the tensile element is unloading from the plastic phase, as shown in Fig. 10(c), w_n is given by

$$w_n = \int \left[\sigma^{\text{crit}} (\varepsilon^{\text{plas}} - \varepsilon^{\text{crit}}) + \frac{1}{2} \sigma_B (\varepsilon_B - \varepsilon^{\text{plas}} + \varepsilon^{\text{crit}}) \right] dV \tag{19}$$

where $\varepsilon^{\text{plas}}$ = strain at the point at which unloading is from a plastic to an elastic phase.

The total strain energy is the summation of all element strain energy:

$$W_s = \sum_{n=1}^{N_e} w_n \tag{20}$$

where N_e = total number of elements.

The damping work is done by a damping force over each particle displacement. Because damping causes energy dissipation, the damping work always points in the opposite direction of the particle velocity, which is given by

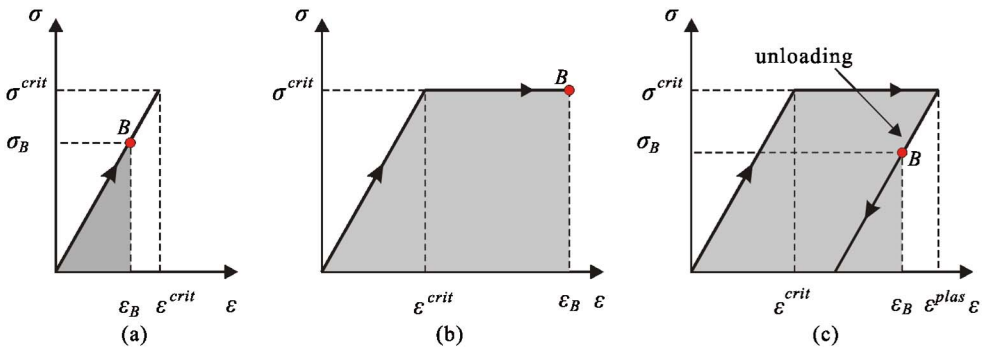

Fig. 10. Element strain energy: (a) elastic phase; (b) plastic phase; (c) unloading phase

J. Struct. Eng. 2011.137:1168-1181.

$$W_d = \sum_{n=1}^{N_p} \mu m_n v_n \Delta_n \tag{21}$$

The external work should be equal to the internal work over the entire simulation time:

$$W_e = W_s + W_k + W_d \tag{22}$$

To verify the energy conservation in the progressive failure process obtained by FPM, a 2D frame structure shown in Fig. 11(a) was analyzed as an example. The material had a Young's modulus $E = 69$ GPa, yield stress $\sigma^{\text{crit}} = 400$ MPa, and density $\rho = 2{,}700$ kg/m^3. The cross-section area of each element was 0.0005 m^2. The time step $\Delta t = 1 \times 10^{-5}$ ms was set for the analysis. A constant load was applied to the two ends of the structure, and it was removed after fracture happened, as shown in Fig. 11(b).

Without Damping

In this case, the damping was not considered. The failure process is shown in Fig. 12. The two ends of the structure were separated at last because of the stress concentrations at these two parts. Consider Member AB, located at one end of the structure, marked in Fig. 12(a). The variations of its element internal force and displacement are shown in Fig. 13. The internal force and displacement first increased linearly. After the yield stress was reached, the element went into the plastic phase. Element AB was separated from the main body of the structure at the point at which fracture happened at $t_f = 0.73$ ms. Although the external load disappeared at that time, the strain energy increased because of decreasing kinetic

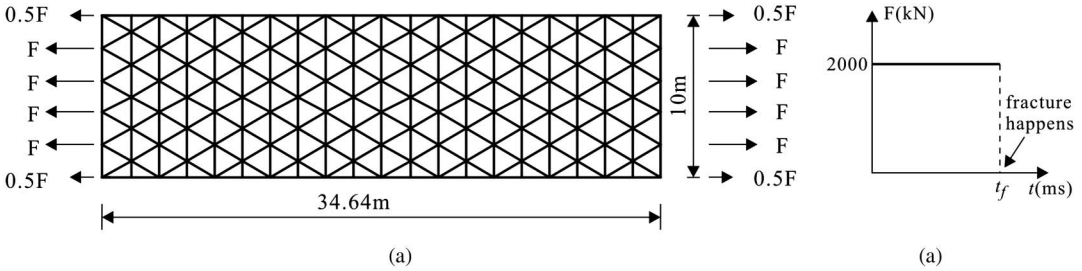

Fig. 11. (a) 2D framed structure; (b) load history

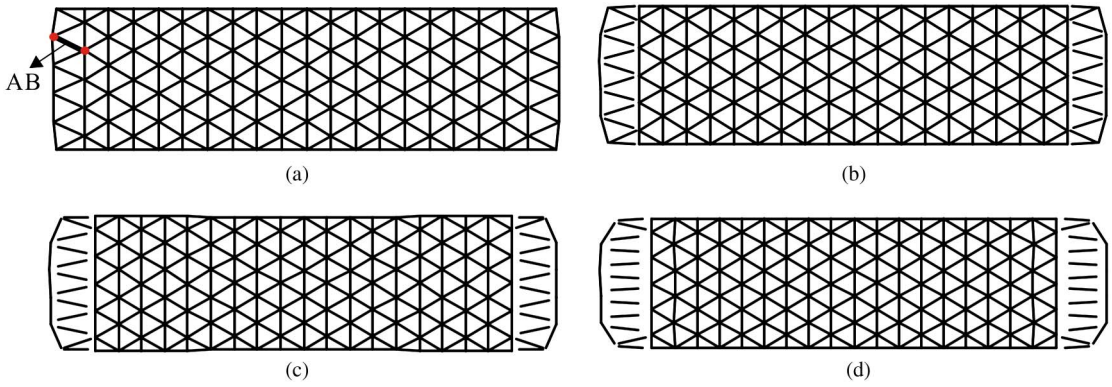

Fig. 12. Failure process of framed structure under constant load: (a) $t = 2.5$ ms; (b) $t = 5$ ms; (c) $t = 7.5$ ms; (d) $t = 10$ ms

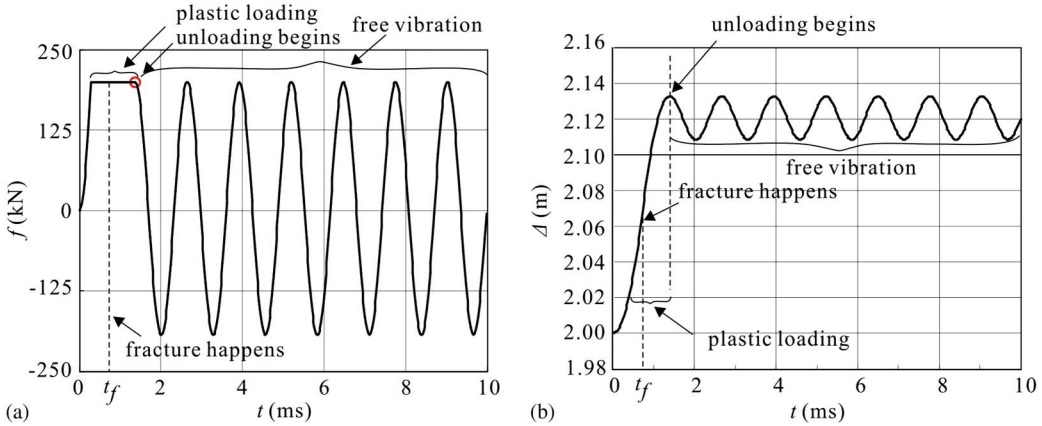

Fig. 13. (a) Internal force; (b) displacement variations of Member AB during failure process without damping

J. Struct. Eng. 2011.137:1168-1181.

energy. Thus, the element was still in plastic loading and the internal force did not decrease immediately. After the internal force unloading in the element happened, this element started free vibration.

As shown in Fig. 14(a), the internal and external energy of Element AB increased at first. After fracture happened at both ends of Element AB, both the kinetic energy and the external work dropped immediately. Two reasons explain this phenomenon. One is the external force is removed at the point at which the fracture happens in the structure. The other is that masses of Particles A and B decrease because of the fracture. Before the fracture happens, the mass of Particle A is equal to half of all element masses connected to Particle A. But after fracture happens, the mass of Particle A is only the half mass of Element AB. The same thing happens to Particle B. Then, the strain energy and kinetic energy transform one another, whereas the total internal energy of Element AB is conserved. The total energy conservation of the entire structure is shown in Fig. 14(b). The total internal energy and the external work are always identical to one another, even after failure.

With Damping

Consider now a damping factor $\mu = 0.5$. The failure process of the structure was almost the same as the situation without damping, which is omitted. But the situation was totally different for energy.

The variations of the internal force and displacement in Element AB are shown in Fig. 15. After the element was separated from the main body of the structure, the element started vibration. Because the damping force dissipated energy, the amplitude of the vibration became smaller and smaller. The kinetic energy disappeared at approximately 100 ms. The plastic deformation could not be recovered. Thus, strain energy existed in the element at last. The total internal energy, including the strain energy, kinetic energy, and damping work, became a constant after the fracture happened. The energy conservation of the entire structure, shown in Fig. 16(b), is also balanced during the failure process.

Progressive Failure Analysis of Truss Structure Under Typhoon Conditions

In this section, a dynamic failure analysis is performed by using FPM to simulate the collapse process of a practical project.

Analyzed Model of FPM

Fig. 17 shows a cantilever truss structure used as the roof of an audience stand at Sanmen, China. Each member of the structure was modeled by a 3D bar element and two particles. The total particle and element numbers were 416 and 1,456, respectively. The material properties of the steel roof were Young's modulus $E = 206$ GPa, yield stress $\sigma^{crit} = 243$ MPa, and density $\rho = 7{,}900$ kg/m^3. The properties of the pipe cross sections used in the structural members are shown in Fig. 18. The columns were concrete-filled steel tubes, 0.6 m in diameter. The properties of the concrete were Young's modulus $E = 31.5$ GPa and density $\rho = 2{,}000$ kg/m^3. Compared to the steel roof, the reinforced concrete columns were very strong, and they remained intact during the typhoon. Therefore, the deformations of these columns were ignored in the analysis, and they were considered to be fixed supports of the roof.

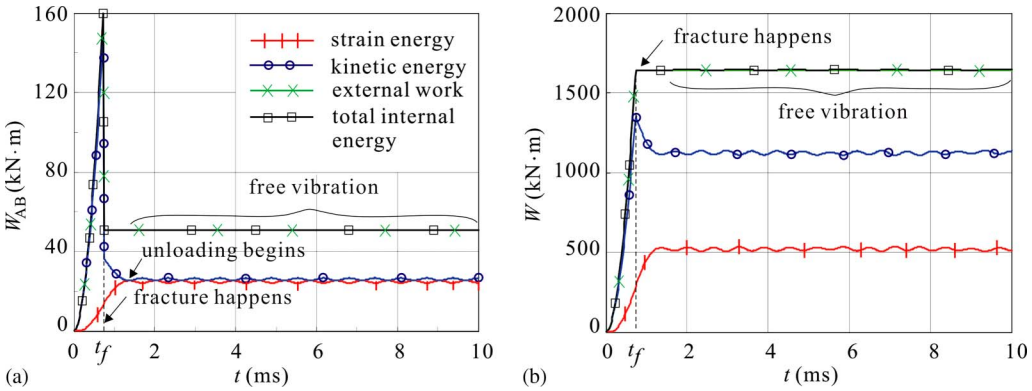

Fig. 14. Energy conservation without damping: (a) Element AB; (b) entire structure

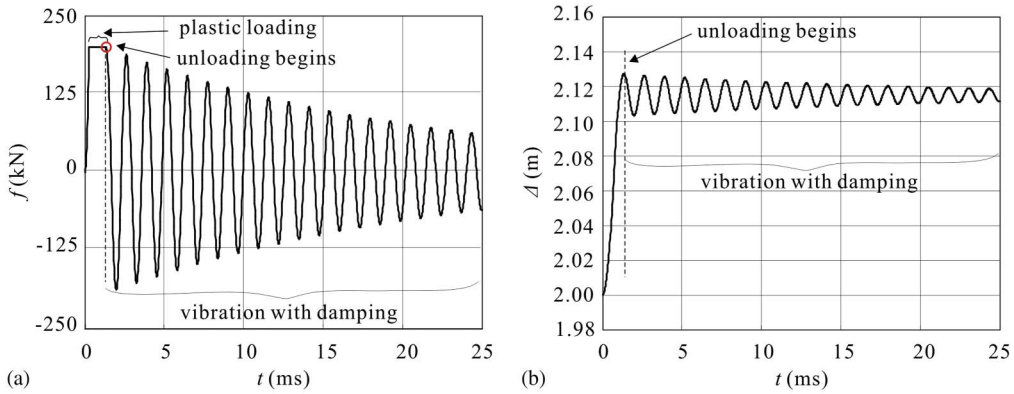

Fig. 15. (a) Internal force; (b) displacement variations of Member AB during failure process with damping

J. Struct. Eng. 2011.137:1168-1181.

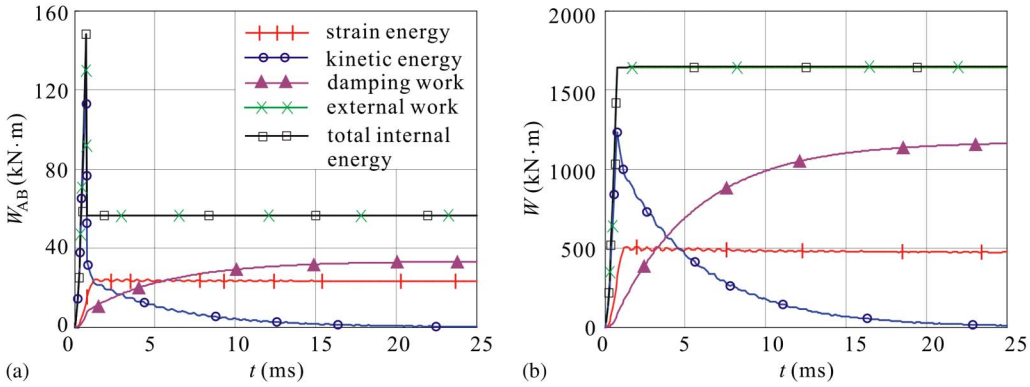

Fig. 16. Energy conservation with damping: (a) Element AB; (b) entire structure

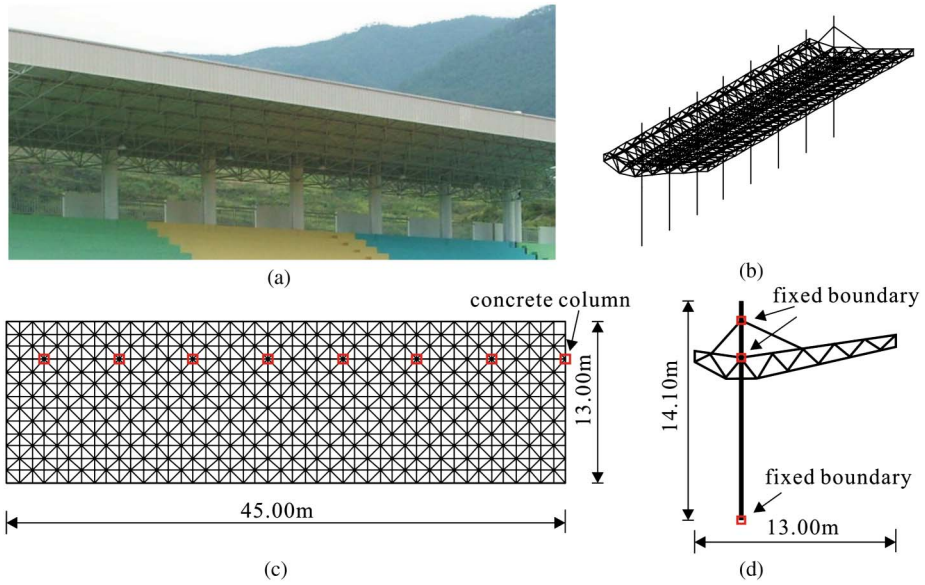

Fig. 17. Cantilever-framed structure: (a) structure in use (Image by Y.Yu); (b) axisymmetric view; (c) plane view; (d) vertical view

Load Conditions

This structure was destroyed by a typhoon in 2005. A typhoon is one kind of the most complicated dynamic loads. Because the failure simulation algorithms are focused on in this paper, wind loads were simplified as constant impact loads in the analysis. The duration of the impact load was 2 ms. According to the weather records, the direction of the typhoon attacking the structure was south to north with an extreme velocity 61.013 m/s, as shown in Fig. 19(a). But the extreme wind velocity used in the design of the structure was only 31.45 m/s on the basis of a 50 years recurrence interval. Therefore, no doubts existed that the structure would collapse under the typhoon. The relationship between the wind pressure, ω, and wind velocity, v, is given by $\omega = v^2/1{,}600$ [Ministry of Housing and Urban-Rural Development (MOHURD) 2002], from which the wind pressure of the typhoon can be determined. Because the windward side of the cantilever was titled 10° upward, and the space under the roof was occupied by stands, the wind on the leeward side was assumed to be blocked and neglected in the analysis. Wind loads were applied to the structure as equivalent distributed loads that were perpendicular to the surface of the roof, as shown in Fig. 19(b).

The design dead and live loads on the roof were 1.3 kN/m^2 and 0.5 kN/m^2, respectively. The initial gravity load was included in the dead load.

Analytical Conditions and Results

The time step $\Delta t = 1 \times 10^{-5}$ s was set in the analysis. The equivalent impact loads were removed at $t = 2$ ms. After that, only the dead and live loads were considered in the system. The damping force of the structure was not considered.

Fig. 20 shows the axial force variations of marked rods in Fig. 18, which could reflect the wave propagation of the dynamic loads and failure states of structural members in the cantilever roof. When $t = 1.92$ ms, the stress of Rod 1 exceeded the elastic limit and went into the plastic plateau; when $t = 2.3$ ms, fracture happened at one end of Rod 1 because of over compression. After that, the internal force of Rod 1 started to fluctuate. Rod 4 had a very similar failure process, but it failed because of over tension. Rods 2, 3, 5, and 6 were adjacent to Rods 1 and 4, respectively. Stresses of both Rod 2 and Rod 5 increased in an elastic phase at the beginning. After fractures happened in Rods 1 and 4, the variation trends of stresses in Rods 2 and 5 changed. Fractures resulted in the unloading of these two rods. Then, their internal forces started to fluctuate.

J. Struct. Eng. 2011.137:1168-1181.

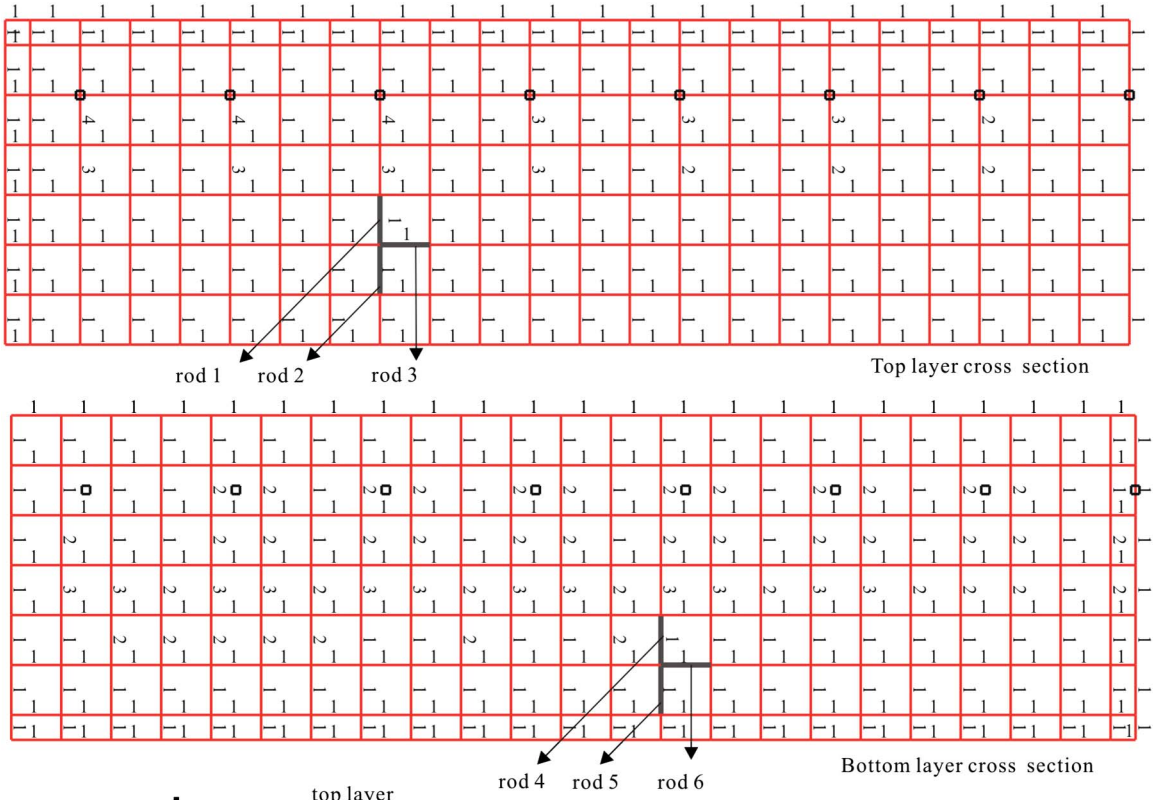

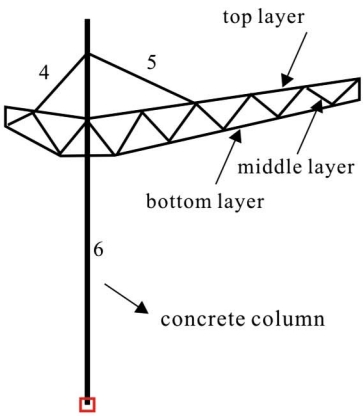

Dimensions of structural members

Section No.	Material	Shape	Cross section (mm)
1	steel	pipe	42×3
2	steel	pipe	48×3.5
3	steel	pipe	60×3.5
4	steel	pipe	75.5×3.75
5	steel	pipe	88.5×4
6	reinforced concrete	round column	Diameter 600
Note: Cross section of all middle layer members is Section No. 1.			

Fig. 18. Cross section of cantilever-framed structure

The stresses of Rods 3 and 6 were very small at the beginning. The fractures of Rods 1 and 4 led to the loading of these two rods. Then, the stresses of Rods 3 and 6 become much larger and started to fluctuate in an elastic phase.

Figs. 21 and 22 show the progressive failure of the structure. At $t = 2.3$ ms, fractures first happened in the top layer members of the cantilever part because of compression. At approximately 2.4 ms, members in the bottom layer were subjected to tensile failures. Part AB of the cantilever structure was then rotated by the effect of the wind about Point A and separated from the main body at last. Although only the axial force in the 3D bar element was considered, the analytical results surprisingly show the shear failure was

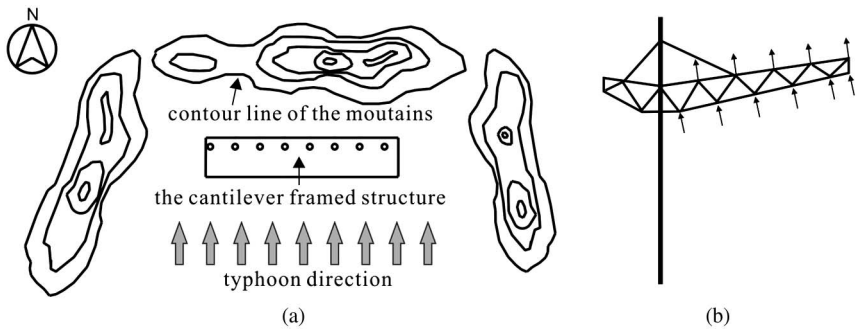

Fig. 19. Typhoon and structure information: (a) wind direction and structural surrounding landform; (b) simplified distributed wind load on structure

J. Struct. Eng. 2011.137:1168-1181.

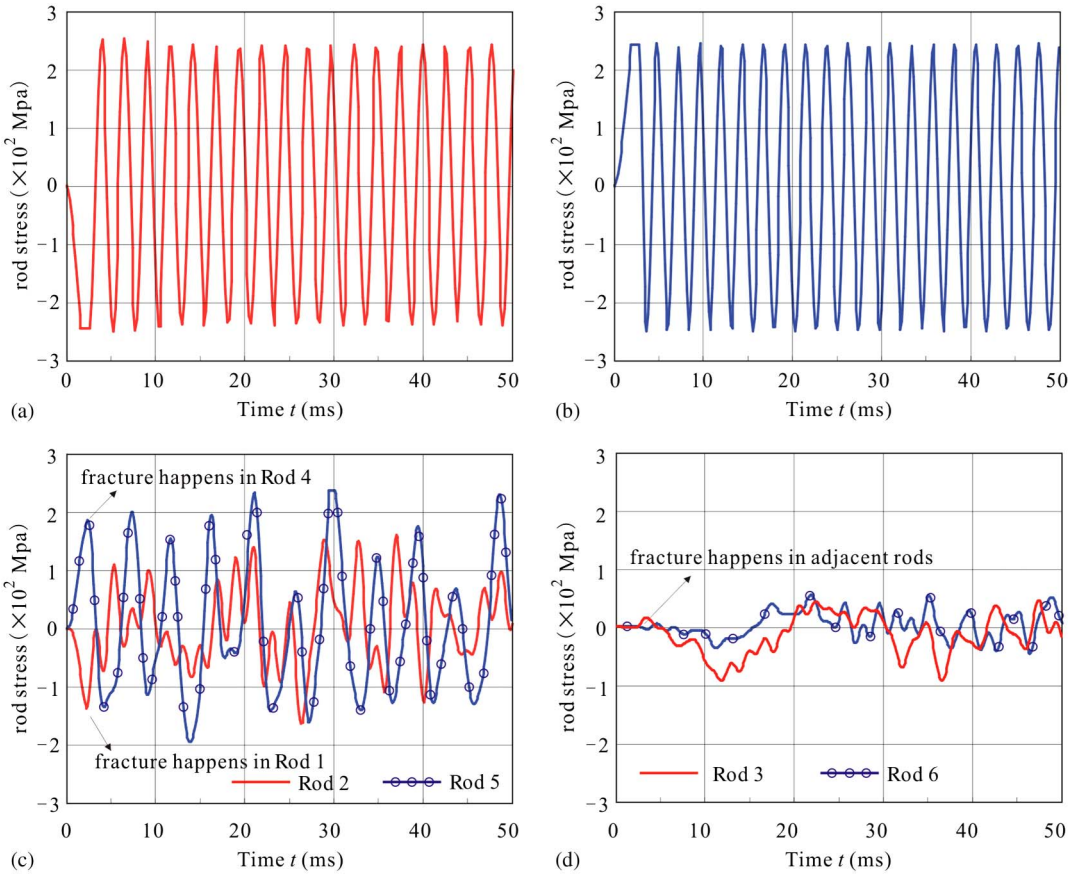

Fig. 20. Variations of rod stresses during fracture process: (a) Rod 1;(b) Rod 4; (c) Rods 2 and 5; (d) Rods 3 and 6

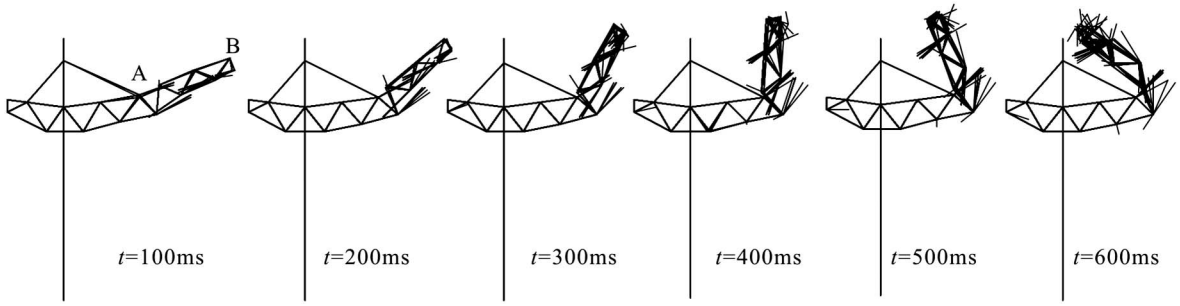

Fig. 21. Vertical view of cantilever structure failure process

the primary failure mode of the structure. The calculation of the failure process for the cantilever structure took approximately 8 s of computer time for a physical time of 0.6 s.

The total energy conservation of the entire structure during the failure process is shown in Fig. 23. Fig. 23(a) shows the details of the energy conservation at the beginning of the fracture. At $t = 2.0$ ms, the impact loads were removed and the structure only had dead and live loads at that point in time. The external work started to decrease at that time, because the direction of gravity was different from the direction of the particle motion, and the live and dead loads did minus work. The kinetic energy decreased immediately because of the disappearing of impact loads, whereas the strain energy continued to increase at this point. At $t = 2.3$ ms, the fracture first occurred. The free ends of the failure members released some strain energy at first. The released strain energy was then changed to kinetic energy; and, so, the kinetic energy stopped decreasing. From then on, the strain energy and kinetic energy transformed to one another, and the value of their summation was identical to the external work.

Fig. 23(b) shows the variation of the structural energy from $t = 0$ to $t = 1{,}200$ ms. The external work and the kinetic energy would increase again, indicating that live and dead loads would change the directions of particle motions and would finally do positive work. As the particle motion was accelerated by gravity, the kinetic energy also increased again. After most of the possible failure happened in the structure, the strain energy vibrated around a stable value. The total energy was conserved during the entire failure process.

Fig. 24 shows damage views of the structure from both the observation of the real failure site and from the analytical results. The comparison of the two results indicates that the collapse simulated by the FPM can catch the basic information of the structure failure.

J. Struct. Eng. 2011.137:1168-1181.

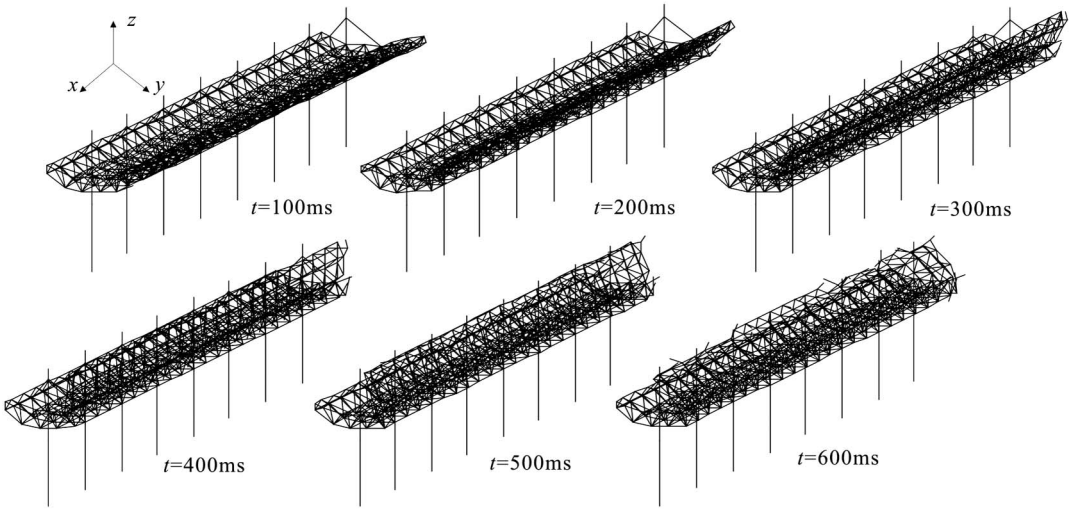

Fig. 22. Axisymmetric view of cantilever structure failure process

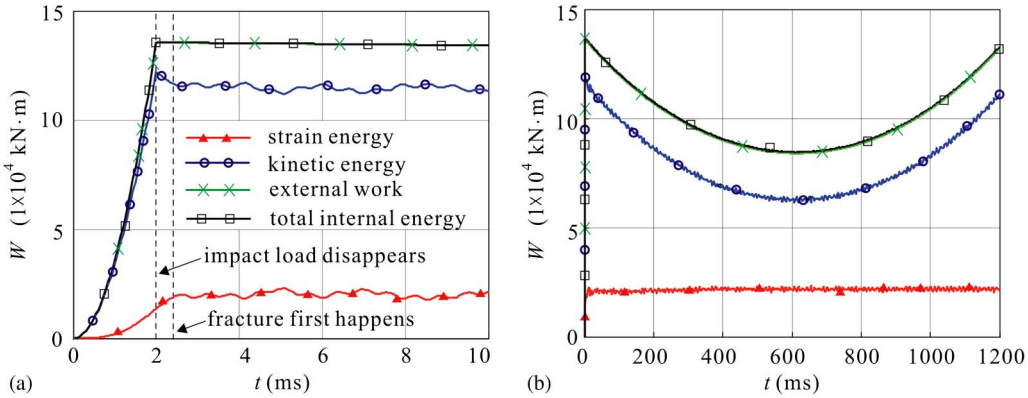

Fig. 23. Energy conservation during failure process of cantilever roof: (a) from $t = 0$ to $t = 10$ ms; (b) from $t = 0$ to $t = 1{,}200$ ms

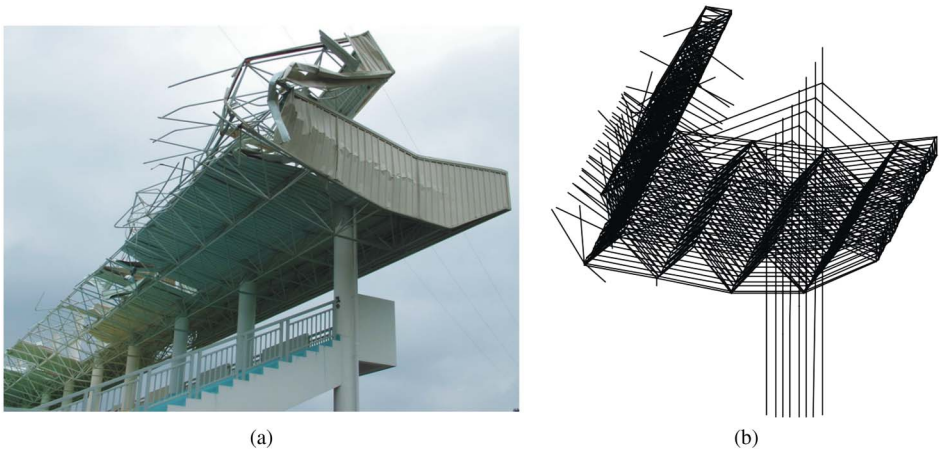

Fig. 24. Damage of cantilever roof: (a) observed (Image by Y.Yu); (b) simulated by using FPM

Conclusion

A general FPM framework for simulating truss structure failure was proposed in this paper. The fundamentals of this method were proposed first. At first glance, the FPM seemed similar to the traditional corotational formulation of frame analysis. However, the differences in evaluating deformation and forces were significant, both in basic concept and procedure. By using a fictitious reverse motion, the structural element was moved to a convected material frame configuration. After evaluating deformation and obtaining internal forces at this configuration, the element was moved back to the original position by a forward motion.

J. Struct. Eng. 2011.137:1168-1181.

In a comparison of traditional approaches for truss analysis, the FPM enforced equilibrium on each particle instead of imposing a global equilibrium of the entire continuous system. No iterations were necessary to follow nonlinear laws, and no matrices were formed or solved in this method. Without any special treatments, the FPM can be used to analyze the nonlinear dynamic behavior of the star dome truss with the same program used in the linear static analysis, which proves the accuracy and generality of this method.

The FPM is advantageous in the simulation of structural failure because particles are free to separate from one another. A simple and straightforward method for detecting and modeling truss structural failure was introduced into the FPM. According to the energy conservation study of a 2D truss, different kinds of energies were balanced during the failure process. This failure simulation algorithm was also used in a practical 3D truss structure failure simulation. From the results, the basic failure mode of the structure, which was quite close to the practical failure image, was observed. If the 3D beam element was developed to simulate this example, more failure details could be caught. Therefore, it is believed that the further development of the FPM can provide engineers with an effective tool to analyze complicated failure problems.

Acknowledgments

The authors are grateful to Professor Ting of Purdue University for his valuable advice during the preparation of this work, including prior access to the vector mechanics. The authors thank Dr. Ivan F. M. Menezes for his invaluable suggestions to this work. The first author would like to thank the Chinese Scholarships Council (CSC) Foundation for students studying abroad. The project is supported by the National High-Tech R&D (863) Program (No. 2007AA04Z441) and the National Natural Science Foundation of China (No. 51108257).

References

Cundall, P. A., and Strack, O. D. L. (1979). "A discrete element model for granular assemblies." *Geotechnique*, 29(1), 47–65.

Driemeier, L., Proenc, S. P. B., and Alves, M. (2005). "A contribution to the numerical nonlinear analysis of three-dimensional truss systems considering large strains, damage and plasticity." *Commun. Nonlinear Sci. Numer. Simul.*, 10(5), 515–535.

Goldstein, H., Poole, C., and Safko, J. (2002). *Classical mechanics*, Addison-Wesley, Cambridge, MA.

Kassimali, A., and Bidhendi, E. (1988). "Stability of trusses under dynamic loads." *Comput. Struct.*, 29(3), 381–392.

Koshizuka, S., Nobe, A., and Oka, Y. (1998). "Numerical analysis of breaking waves using the moving particle semi-implicit method." *Int. J. Numer. Methods Fluids*, 26(7), 751–769.

Krenk, S. (2006). "Energy conservation in Newmark based time integration algorithms." *Comput. Methods Appl. Mech. Eng.*, 195(44–47), 6110–6124.

Leu, L. J., and Yang, Y. B. (1990). "Effects of rigid body and stretching on nonlinear analysis of trusses." *J. Struct. Eng.*, 116(10), 2582–2598.

Lewis, W. J. (1984). "Dynamic relaxation analysis of the non-linear static response of pretensioned cable roofs." *Comput. Struct.*, 18(6), 989–997.

Lynn, K. M., and Isobe, D. (2007a). "Finite element code for impact collapse problems." *Int. J. Numer. Methods Eng.*, 69(12), 2538–2563.

Lynn, K. M., and Isobe, D. (2007b). "Structural collapse analysis of framed structures under impact loads using ASI-Gauss finite element method." *Int. J. Impact Eng.*, 34(9), 1500–1516.

Ministry of Housing and Urban-Rural Development (MOHURD). (2002). *China load code for the design of building structures*, China Building Industry Press, Beijing.

Monaghan, J. J. (1992). "Smoothed particle hydrodynamics." *Annu. Rev. Astron. Astrophys.*, 30(1), 543–574.

Oliver, K.-H., and Hermann, G. M. (2005). "Least squares finite element methods for fluid-structure interaction problems." *Comput. Struct.*, 83(2–3), 191–207.

Onate, E., Idelsohn, S. R., Pin, F. D., and Aubry, R. (2004). "The particle finite element method: An overview." *Int. J. of Comput. Methods*, 1(2), 267–307.

Papadrakakis, M. (1981). "Post-buckling analysis of spatial structures by vector iteration methods." *Comput. Struct.*, 14(5–6), 393–402.

Shih, C., Wang, Y.-K., and Ting, E. C. (2004). "Fundamentals of a vector form intrinsic finite element. Part III: Convected material frame and examples." *J. Mech.*, 20(2), 133–143.

Tavarez, F. A., and Plesha, M. E. (2007). "Discrete element method for modelling solid and particulate materials." *Int. J. Numer. Methods Eng.*, 70(4), 379–404.

Ting, E. C., Shih, C., and Wang, Y.-K. (2004). "Fundamentals of a vector form intrinsic finite element. Part, I. Basic procedure and a plane frame element." *J. Mech.*, 20(2), 113–122.

Wu, T. Y., Lee, J. J., and Ting, E. C. (2008). "Motion analysis of structures (MAS) for flexible multibody systems: Planar motion of solids." *Multibody Syst. Dyn.*, 20(3), 197–221.

Wu, T. Y., and Ting, E. C. (2008). "Large deflection analysis of 3D membrane structures by a 4-node quadrilateral intrinsic element." *Thin-Walled Struct.*, 46(3), 261–275.

Wu, T. Y., Wang, R. Z., and Wang, C. Y. (2006). "Large deflection analysis of flexible planar frame." *J. Chin. Inst. Eng.*, 29(4), 593–606.

Yu, Y. (2010). *Progressive collapse of space steel structures based on the finite particle method [D]*, Zhejiang University Press, Hangzhou, China.

Yu, Y., and Luo, Y. (2009a). "Finite particle method for kinematically indeterminate bar assemblies." *J. Zhejiang Univ. Sci. A*, 10(5), 669–676.

Yu, Y., and Luo, Y. (2009b). "Motion analysis of deployable structures based on the rod hinge element by the finite particle method." *Proc. Inst. Mech. Eng., Part G*, 223(7), 955–964.

Zhang, Z. Y., Paulino, G. H., and Celes, W. (2007). "Extrinsic cohesive modelling of dynamic fracture and microbranching instability in brittle materials." *Int. J. Numer. Methods Eng.*, 72(8), 893–923.

J. Struct. Eng. 2011.137:1168-1181.